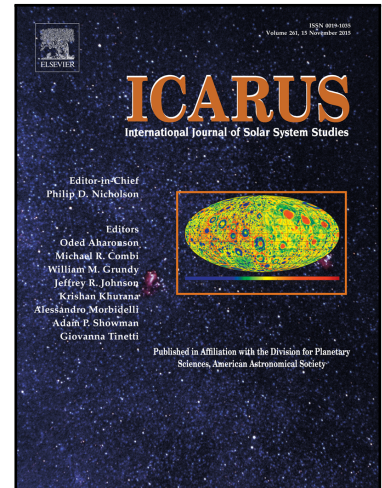


# Accepted Manuscript



An improved JPL Mars Gravity Field and Orientation from Mars Orbiter and Lander Tracking Data

Alex. S. Konopliv , Ryan S. Park , William M. Folkner

PII: S0019-1035(16)00130-5  
DOI: [10.1016/j.icarus.2016.02.052](https://doi.org/10.1016/j.icarus.2016.02.052)  
Reference: YICAR 11971

To appear in: *Icarus*

Received date: 28 October 2015  
Revised date: 23 February 2016  
Accepted date: 29 February 2016

Please cite this article as: Alex. S. Konopliv , Ryan S. Park , William M. Folkner , An improved JPL Mars Gravity Field and Orientation from Mars Orbiter and Lander Tracking Data, *Icarus* (2016), doi: [10.1016/j.icarus.2016.02.052](https://doi.org/10.1016/j.icarus.2016.02.052)

This is a PDF file of an unedited manuscript that has been accepted for publication. As a service to our customers we are providing this early version of the manuscript. The manuscript will undergo copyediting, typesetting, and review of the resulting proof before it is published in its final form. Please note that during the production process errors may be discovered which could affect the content, and all legal disclaimers that apply to the journal pertain.

An improved JPL Mars Gravity Field and Orientation from Mars Orbiter and Lander Tracking Data

Alex. S. Konopliv<sup>a</sup>\*, Ryan S. Park<sup>a</sup>, William M. Folkner<sup>a</sup>

<sup>a</sup>Jet Propulsion Laboratory, California Institute of Technology, 4800 Oak Grove Dr., Pasadena, CA 91109 USA

\*Corresponding author: E-mail: Alex.Konopliv@jpl.nasa.gov

### Abstract

The Mars gravity field resolution is mostly determined by the lower altitude Mars Reconnaissance Orbiter (MRO) tracking data. With nearly four years of additional MRO and Mars Odyssey tracking data since the last JPL released gravity field MRO110C and lander tracking from the MER Opportunity Rover, the gravity field and orientation of Mars have been improved. The new field, MRO120D, extends the maximum spherical harmonic degree slightly to 120, improves the determination of the higher degree coefficients as demonstrated by improved correlation with topography and reduces the uncertainty in the corresponding Mars orientation parameters by up to a factor of two versus previously combined gravity and orientation solutions. The new precession solution is  $\dot{\psi} = -7608.3 \pm 2.1$  mas/yr and is consistent with previous results but with a reduced uncertainty by 40%. The Love number solution,  $k_2 = 0.169 \pm 0.006$ , also shows a similar result to previous studies.

### 1. Introduction

The initial global high-resolution Mars gravity models were determined using the Mariner 9 and Viking Orbiter S-band Doppler tracking data obtained 1969-1979 [Smith *et al.*, 1993; Konopliv and Sjogren, 1995]. However, due to the high elliptical orbits the resolution of the gravity field was not uniform. The first completely uniform global

gravity field results occurred with Mars Global Surveyor (MGS) with its nearly circular low altitude (~380-km periapse) polar frozen orbit and more accurate X-band Doppler tracking data. Initially, multiple independent centers produced high-resolution gravity solutions that were determined from the MGS data [Smith *et al.*, 1999; Lemoine *et al.*, 2001; Yuan *et al.*, 2001; and Konopliv *et al.*, 2006; Marty *et al.*, 2009]. The later solution MGS95J includes many years of Mars Odyssey X-band tracking data in a similar orbit as MGS and an improved Mars orientation model that includes Mars nutation.

The Mars Reconnaissance Orbiter (MRO) spacecraft began collecting X-band tracking data on the Mars gravity field in August 2006 [Zuber *et al.*, 2007]. The lower altitude (255-km periapse) polar orbit significantly improved the global average resolution of the gravity field from about harmonic degree 70 to harmonic degree 90. The initial JPL MRO based gravity solutions included MRO95A, MRO110B, MRO110B2 as described in Konopliv *et al.* [2011], and the n=110 models included MRO tracking data to October 2008. An additional model MRO110C included several more years of MRO data to May 2011. All MRO models are archived with the Planetary Data System (PDS) Geosciences Node (<http://geo.pds.nasa.gov/>) under the MRO gravity science archive.

A new solution, MRO120D, with MRO tracking data to end of April 2015 is presented in this paper. The additional four years of MRO tracking data has improved the higher degree gravity coefficients. Also the additional 3 years plus of Mars Odyssey data together with newly included four months of Mars Exploration Rover (MER) Opportunity data in the Mars gravity solution improves the Mars orientation solution.

Spacecraft	Begin time mm-dd-yyyy	End time mm-dd-yyyy	Number of arcs	Number of 1-way Doppler	Number of 2-way Doppler	Number of 3-way Doppler	Number of range
------------	-----------------------	---------------------	----------------	-------------------------	-------------------------	-------------------------	-----------------

MGS	03-28-1998	09-23-2006	611	3,844,863	4,139,924	329,404	170,657
Odyssey	01-11-2002	01-03-2015	1044		9,858,907	2,250,415	492,670
MRO	08-30-2006	04-30-2015	709		8,802,946	1,159,608	41,354
Pathfinder	07-04-1997	10-07-1997	1		6726		91
Viking Lander	07-21-1976	11-13-1982	1		12991		1165
MER Opportunity	01-02-2012	05-02-2012	1		1387		

Table 1. Summary of the number of Doppler and range tracking observations used in the MRO120D gravity solution for the Mars orbiters (MGS, Odyssey, and MRO) and landers (Pathfinder, Viking Lander and MER Opportunity).

## 2. Spacecraft Orbiter and Lander Tracking Data

Multiple tracking data sets are included in the development of the Mars gravity field. The Mars orbiter Doppler tracking data are the primary observables for determining the spherical harmonic gravity coefficients, but they also contribute strongly to the Mars orientation solution together with the Mars lander tracking data. The range tracking data are also of primary importance in the determination of the Mars ephemeris and other parameters such as asteroid masses [Konopliv *et al.*, 2011]. The DE430 planetary ephemeris [Folkner *et al.*, 2014] was used for this study and includes range data from the Mars orbiters through 2012. The primary data sets from Mars orbiters included in this gravity solution are the entire MGS mapping mission data set from the mission start to 2015 for the Mars Odyssey and MRO data sets. Tracking data from the MAVEN mission is not yet included. All orbiter data process Doppler data as 10-s sample times. The lander tracking data includes Mars Pathfinder, Viking Lander and MER, where all data is processed as 60-s count times. The orbiter and lander data sets for this solution (Table 1) are the same as for the MRO110B and MRO110C solutions except additional years of MRO and Mars Odyssey tracking data are included as well as the MER tracking data.

The Mars Odyssey displays the best tracking data accuracy of the three orbiter missions [e.g. Fig 2 of *Konopliv et al.*, 2011] near 0.03 mm/s at 10-s sample time. The MGS tracking data is known to be noisier due to deployed antenna vibration, whereas the MRO increase in noise is related to the Ka-band hardware failure, which occurred during spacecraft cruise to Mars. The noise in the MRO Doppler data is inherent in the small deep space transponder (SDST-1) and is dominated by a near single frequency that varies in period between 4 and 5 seconds over the course of the mission. The noise is noticeably reduced for the limited time when the backup SDST-2 is used beginning in March 2014. This study successfully reduces this anomaly by removing one single frequency periodic term every 5 minutes from the Doppler residuals for SDST-1. Over each interval, a periodogram determines the anomalous frequency with the maximum amplitude in the MRO 1-sec residuals. A single frequency cosine and sine term (whose period and amplitude varies over the mission, typically 0.3-0.4 mm/s) is removed from the 1-sec observables and the new Doppler data is then compressed to 10-sec. Once corrected, the 10-sec MRO Doppler accuracy improves by up to 40% from 0.05 mm/s to 0.03 mm/s for better Mars-Earth-Sun angles where the solar plasma noise contribution is smaller. Although the Doppler noise is improved, the overall improvement in the gravity field due to this particular correction is small.

All three orbiters have about 1 mm/s corrections in the Doppler for antenna motion as the high-gain antenna remains directed to the Earth as the instruments are generally nadir pointed. The motion of the antenna phase center with respect to the spacecraft center-of-mass is modeled using the PDS provided antenna gimbal angles [Semenov et al., 1998, 2004; Semenov and Acton, 2007] and spacecraft attitude. All

orbiter and lander Doppler and range data are calibrated at each Deep Space Network (DSN) complex for daily Earth media corrections that include dry and wet troposphere and ionosphere calibrations based upon GPS measurements. The orbiter Doppler data are weighted according to the RMS of each DSN pass with data arcs near solar conjunction deleted for average RMS values greater than about 0.2 mm/s for the 10-s integration times. As with previous studies, this corresponds to deleting data arcs with a Sun-Earth-Probe angle less than  $\sim 10^\circ$ .

The lander tracking data includes the same Viking Lander S-band and Mars Pathfinder X-band Doppler and range data as previous studies [Folkner *et al.*, 1997; Konopliv *et al.*, 2011; Kuchynka *et al.*, 2014]. The Viking Doppler data extends from July 1976 to December 1978 and Mars Pathfinder data from July 1997 to October 1997. Individual Doppler are generally correlated with other Doppler measurements, because solar plasma cause effects with time scales longer than the time between measurements. As a result, the power spectral density of the Doppler measurement residuals is not flat ('white') but follows a  $f^{8/3}$  phase power law [Woo and Armstrong, 1979]. For the Viking and Pathfinder data, we use knowledge of the power spectral density to 'whiten' the measurements, creating a time series that is uncorrelated, in the same manner as done by Kuchynka *et al.* [2014]. Weighting the whitened data at their RMS correctly accounts for the correlations in the original data. As in Kuchynka *et al.* [2014], we also exclude Viking Lander data near solar conjunction or for a Sun-Earth-Mars angle less than about  $15^\circ$ . This was not done in the previous studies of Konopliv *et al.* [2006] and Konopliv *et al.* [2011].

The new MER Opportunity X-band Doppler tracking data was acquired when the rover was stationary during Martian winter. The MER data set is the same as processed by *Kuchynka et al.* [2014] and includes 58 X-band direct to Earth tracking passes using the MER high gain antenna from January 2015 to May 2015 that occur typically every two days. The MER data occurs during favorable Sun angles with diminished solar plasma noise. For this reason the Doppler observables are not treated as correlated but are weighted at a looser 0.12 mm/s as in *Kuchynka et al.* [2014].

#### **4. Spacecraft Force Modeling and Estimation Technique**

The determination of the gravity field and orientation follows the same process of our previous studies [e.g., see *Yuan et al.*, 2001; *Konopliv et al.*, 2006; *Konopliv et al.*, 2011; *Konopliv et al.*, 2013]. The orbiter data, as before, are processed in time intervals (or data arcs) of mostly four day lengths where local parameters of spacecraft state, solar pressure factors, atmospheric density corrections, angular momentum desaturation maneuver corrections, and measurement biases are estimated using a square-root information weighted least squares filter or SRIF [*Lawson and Hanson*, 1995; *Bierman*, 1977].

The atmospheric density corrections include four parameters per orbit for MRO and once per orbit for MGS and Mars Odyssey. The uncertainties in the drag constraint allow for about 50% variation in density for MRO and about 25% for the higher MGS and Mars Odyssey orbiters from a priori density values. The angular momentum desaturation maneuvers include three small delta-velocity corrections (generally <0.03 mm/s) for each event along with a scaling factor on the a priori thrust model for all maneuvers in the arc. As in previous studies, the solar pressure force consists of three

scale factors; one in the probe-Sun direction with an uncertainty of about 5% and two normal to that direction with a smaller 2% uncertainty of the overall force. We also note that we do not estimate any empirical forces (along-track constant, per rev or otherwise).

All the local arcs (with the quantity listed in Table 1) are then combined using a similar technique described by *Kaula* [1966] using partitioned normal matrices, and is equivalent to solving for the global parameters plus local parameters of all arcs to determine the global parameters. The global parameters include the static gravity field to degree and order 120, the seasonal gravity field changes in normalized  $\bar{J}_3$ , the mass parameter of Mars, Phobos, and Deimos, the tidal Love number  $k_2$ , the Mars orientation epoch pole longitude, obliquity, and rates, Mars rotation rate, seasonal corrections to spin, and specular and diffuse corrections for spacecraft solar arrays. Since the seasonal changes in the even zonal coefficients are not easily detected, the  $\bar{J}_2$  changes expected from the mass exchange between the polar ice caps are fixed to a periodic model based upon the NASA Ames global atmospheric circulation model.

In our previous study [*Konopliv et al.*, 2011] we showed that the solar pressure model for Mars Odyssey had a significant effect on the estimation of  $k_2$ , which is determined from the secular drift in orbit inclination [*Yoder et al.*, 2003]. This is due to the near face-on geometry of the orbit plane as viewed from the Sun and grazing occultations with the Mars atmosphere. The solar pressure force was reduced because of dust in the Mars atmosphere during the occultations. In *Konopliv et al.* [2011], these effects were accounted for by extending dust shadowing of the spacecraft to about 40-km above the surface. In our current study, we account for changes in the solar pressure model instead by normalizing the solar array power output readings from the spacecraft

telemetry and then scaling the solar pressure force. Both techniques remove anomalous out-of-plane orbit accelerations that affect the  $k_2$  estimate. Fig. 1 shows an example of the Mars Odyssey telemetry power data for one arc, where the solar array power output has been normalized for solar array pointing (cross-sectional area toward the Sun) and spacecraft distance from the Sun. The power is shown as a function of the angle of the orbit from the equator  $\theta$  (argument of periapse plus true anomaly). The spacecraft is at the equator for angles of  $\theta=0^\circ$  and  $180^\circ$  and over the poles for  $\theta=90^\circ$  and  $270^\circ$ . A correction is also applied after exiting occultation ( $\theta \approx 90^\circ$ ) because of solar array heating effects. The average power over the four days (red curve) represents the signature applied to the solar pressure model after normalization.

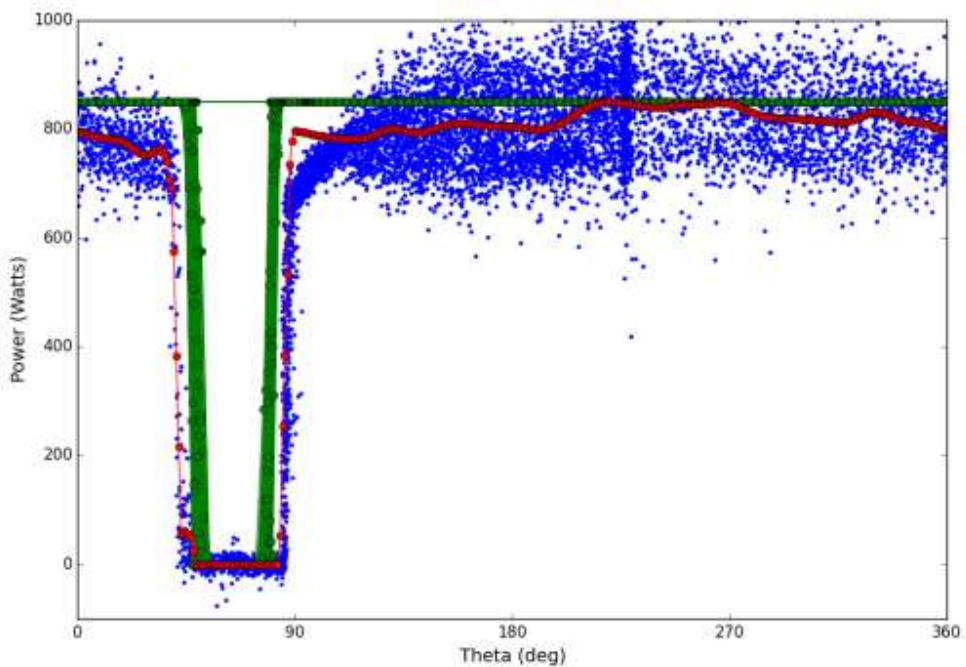


Figure 1. An example of the solar power output for Mars Odyssey (blue dots) based upon the spacecraft telemetry for one 4-day arc beginning July 10, 2005 versus the angle from

the equator  $\theta$ . The red curve shows the average fit of the power. The green curve shows the occultation based upon the shape of Mars. As one can see, power is lost (red or blue) before occultation predicted by the shape of Mars. This is due to dust in the atmosphere. If one increases the radius of Mars by 40-km, then the green curve matches the red curve.

The Mars gravitational potential  $U$  is modeled by a spherical harmonic expansion in the body-fixed reference frame with normalized coefficients  $(\bar{C}_{nm}, \bar{S}_{nm})$  and is given by [e.g., *Heiskanen and Moritz, 1967; Kaula, 1966*]

$$U = \frac{GM}{r} + \frac{GM}{r} \sum_{n=2}^{\infty} \sum_{m=0}^n \left( \frac{R_e}{r} \right)^n \bar{P}_{nm}(\sin \phi) [\bar{C}_{nm} \cos(m\lambda) + \bar{S}_{nm} \sin(m\lambda)]$$

where  $GM$  is the gravitational constant times the mass of the central body,  $n$  is the degree,  $m$  is the order,  $\bar{P}_{nm}$  are the fully normalized associated Legendre polynomials,  $R_e$  is the reference radius of the body (3396 km),  $\phi$  is planetocentric latitude, and  $\lambda$  is the east longitude. The gravity coefficients are normalized such that the integral of the harmonic squared equals the area of a unit sphere, and are related to the unnormalized coefficients as [*Kaula, 1966; Lambeck, 1988*]

$$\begin{pmatrix} C_{nm} \\ S_{nm} \end{pmatrix} = \left[ \frac{(n-m)!(2n+1)(2-\delta_{0m})}{(n+m)!} \right]^{1/2} \begin{pmatrix} \bar{C}_{nm} \\ \bar{S}_{nm} \end{pmatrix} = f_{nm} \begin{pmatrix} \bar{C}_{nm} \\ \bar{S}_{nm} \end{pmatrix}$$

The corresponding normalized Legendre polynomials  $\bar{P}_{nm}$  are thus related to the unnormalized polynomials  $P_{nm}$  by  $P_{nm} = \bar{P}_{nm} / f_{nm}$ . The gravity coefficients are partly constrained with a Kaula power law constraint beginning at degree 80 (similar to Konopliv et al., 2011).

The Mars orientation model follows the model presented in *Folkner et al. [1997]* for the determination of Mars precession using the Mars Pathfinder Lander tracking data.

The orientation model parameters were updated with Mars orbiting data in addition to lander data by *Konopliv et al.*, [2006] with the MGS95J gravity field and *Konopliv et al.* [2011] with the MRO110B gravity field. The orientation was then additionally updated using the orbiter data from the MRO110C gravity solution together with the previous lander data and the stationary MER Opportunity tracking data during the Mars winter [Kuchynka et al., 2014]. The parameters that are part of the Mars orientation definition are shown in Fig. 2. In our analysis and as in previous studies, we estimate Mars precession  $\dot{\psi}_o$ , obliquity rate  $\dot{I}_o$ , spin rate  $\dot{\phi}_o$ , epoch angle values ( $\psi_o, I_o, \phi_o$ ), and annual to 4<sup>th</sup> annual seasonal spin changes ( $\phi_{cj}$  for cosine amplitudes and  $\phi_{csj}$  for sine amplitudes, j=1,4) due to the polar icecap mass exchange, but the Mars nutation contributions are held fixed due to lack of sensitivity to these terms.

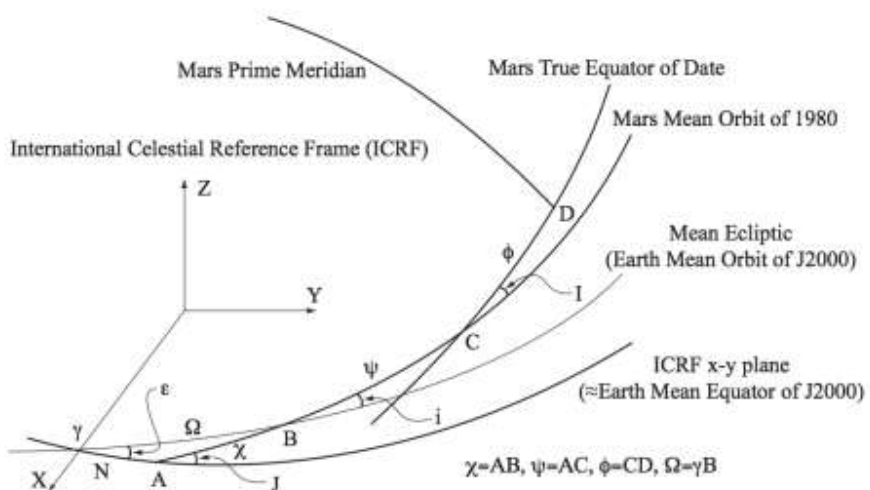


Figure 2. The Mars orientation model parameters. The angles shown are used for conversion from the International Celestial Reference Frame (ICRF) to the Mars body-fixed coordinate frame. Contributions to the angles from precession, nutation and seasonal periodic spin are given in *Konopliv et al.*, 2006.

In our previous studies [*Konopliv et al.*, 2011], we selected the epoch location of the prime meridian  $\phi_0$  to match the original prime meridian location at the J2000 epoch as specified by the IAU convention [*Archinal et al.*, 2011]. In this study we follow the convention of Kuchynka et al. [2014] that fixes the longitude of the Viking Lander 1 to be  $-47.95137^\circ$  as our definition of the prime meridian. We then estimate  $\phi_0$ .

The contributions of the orbiter versus the lander data are combined using a different procedure than the previous studies. For our prior gravity solutions [*Konopliv et al.*, 2006; *Konopliv et al.*, 2011], we directly combined the orbiter and lander data where each was approximately weighted by the RMS of the data. In those studies, the formal uncertainties of the orientation parameters were then scaled up by a factor of 15 to represent realistic errors. This factor was determined by comparing solutions using different subsets of data and assumptions. We now model the Viking and MPF lander data as correlated (and then remove the correlations by whitening) as mentioned above and we also rescale each orbiter (MGS, Mars Odyssey and MRO) entire mission square-root information matrix (SRIF) to achieve realistic errors for the orientation parameters and long-wavelength gravity coefficients. The scaling is based upon differences of the gravity and orientation solution with previous solutions [*Konopliv et al.*, 2006; *Konopliv et al.*, 2011, Kuchynka et al., 2014], model assumptions, and solutions from different data subsets. The Mars Odyssey and MGS SRIF scaling begins at 10 for the orientation parameters and degree 2 gravity harmonics and tapers to one at harmonic degree 40. MRO is similar but begins with a scale of 15 due to the likelihood of increased atmospheric drag errors. As a result, the solution uncertainties no longer need to be increased and represent realistic errors. Changes in the solution with the scaled SRIFs

relative to the unscaled SRIF solution are significantly less than the uncertainties from the scaled solution. Thus there is no need for an iterative process on the scaling factors.

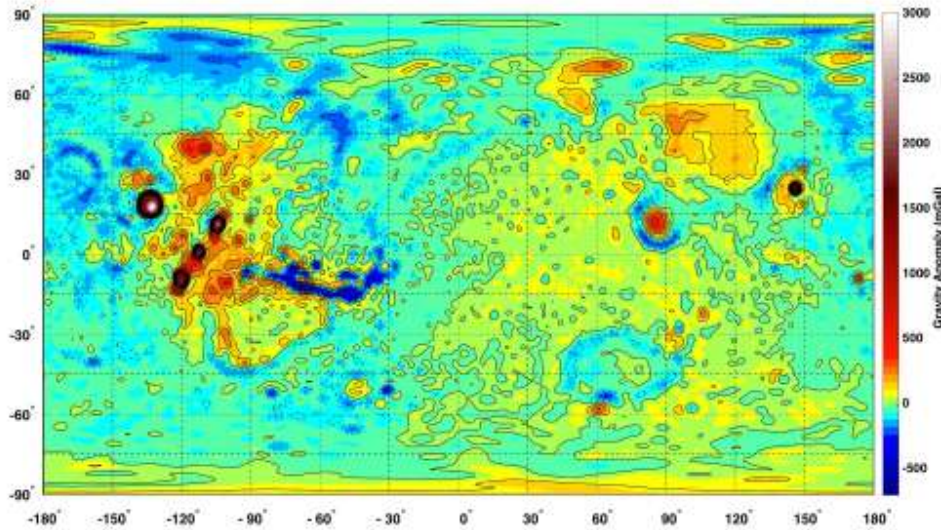


Figure 3. The MRO120D gravity field anomaly truncated at degree 95. This shows the magnitude of the gravity acceleration on the Mars areoid minus the gravity from a reference ellipsoid ( $a_e=3397$  km,  $1/f=196.9$ ). The maximum amplitude is 3135 mGals for Olympus Mons and the minimum is -695 mGals for Valles Marineris.

## 5. Gravity and orientation results

Although the new gravity field MRO120D is determined to harmonic degree 120, the actual global resolution is close to degree 95, where the average uncertainty in the coefficients nearly equals the coefficient magnitude. For this reason, the new gravity field is shown in Fig. 3 as the gravity anomaly with the field truncated to degree 95. We estimate the gravity field to a higher degree 120 since some regions (south pole in particular) have higher resolution, and the orbit determination is sensitive to the near sectoral terms extended to higher degree. The improvement of the gravity spectrum compared to previous solutions is evident in Fig. 4 and the improvement in resolution is mostly due to the additional four years of MRO tracking data. The MRO120D

unconstrained solution deviates from the expected spectrum (shown by the power law  $8.5 \times 10^{-5}/n^2$ ) 5 to 10 degrees later than the previous solution MRO110B. The actual power constraint applied for  $n > 80$  to MRO120D is about 50% looser than the observed spectrum  $8.5 \times 10^{-5}/n^2$ , as noted by the higher uncertainties at the end of the spectrum. The differences in the spectrum between the latest two solutions MRO120D and MRO110C give differences on the surface of up to 85 mGals. The amplitudes of the Tharsis volcanoes between the two solutions, for example, change at most by 20-30 mGals versus the total 2000-3000 mGals amplitude.

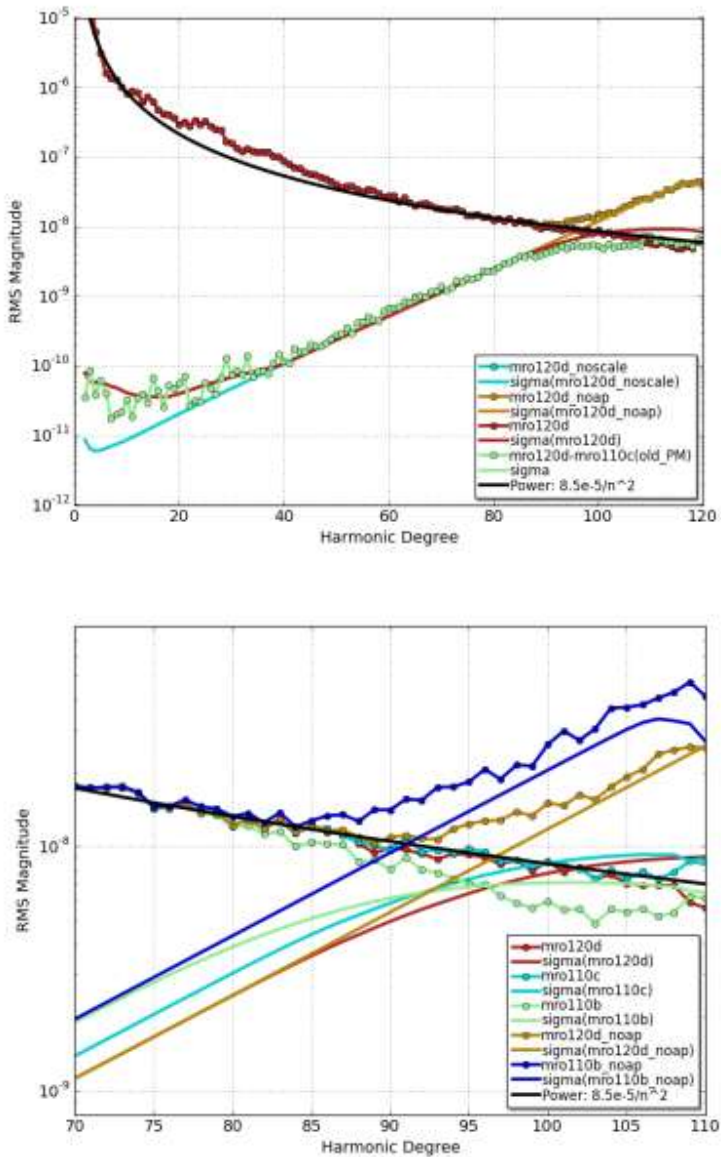
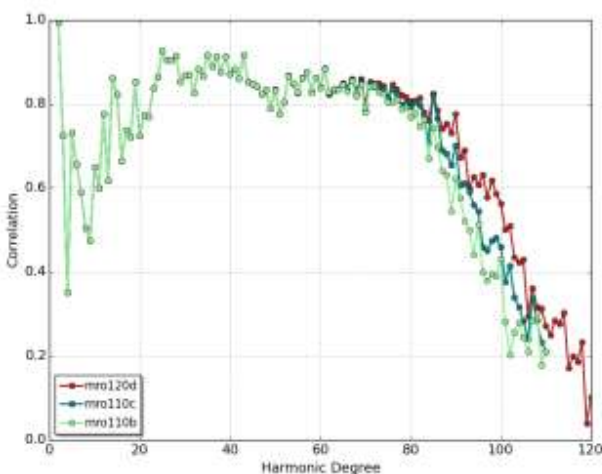


Figure 4. (a) The full gravity spectrum for the MRO120D gravity field with a Kaula power constraint applied to harmonic degrees greater than 80, the gravity solution with out any power a priori constraint (“mro120d\_noap”), and the solution where the orbiter SRIF matrices are not scaled (“mro120d\_noscale”). Note “mro120d\_noap” and “mro120d\_noscale” are nearly identical except for the highest degrees. RMS differences are also shown with the previous MRO110C solution. (b) The higher degree spectra for the MRO120D, MRO110C, and MRO110B (Konopliv et al., 2011) gravity solutions and the unconstrained (no Kaula power rule applied) solutions MRO120D (“mro120d\_noap”) and MRO110B (“mro120b\_noap”).

The effect of the scaled orbiter SRIF matrices is also evident on the gravity error spectrum in Fig. 4a (“mro120d” vs. “mro120d\_noscale”). The original gravity error spectrum without scaling (“mro120d\_noscale”) is overly optimistic for the low degree harmonics and orientation parameters as shown by the difference between the MRO120D and MRO110C solutions. In this difference, MRO120D was determined without scaling and using the same prime meridian as MRO110C, otherwise differences are larger. The newly scaled SRIFs were chosen to match this difference. The corresponding covariance and uncertainties for MRO120D now represent realistic errors whereas previous solutions required scaling the covariance and errors.



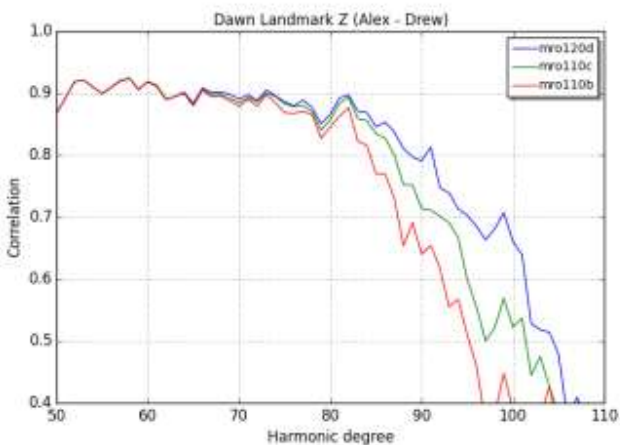


Figure 5. (a) Global and (b) local correlations and of Mars gravity fields MRO120D, MRO110C and MRO110B with the Mars topography. The local correlation is for an 18 degree spherical cap over the Ascraeus Mons volcano in the Tharsis region. The correlation was generated using SHTOOLS (Mark Wieczorek, <http://shtools.ipgp.fr>)

The 5 to 10 degree improvement in the gravity field is also shown in the global correlation with topography [Smith *et al.*, 2001] (Fig. 5a) and with the local correlation example over the Ascraeus Mons volcano in the Tharsis region (Fig. 5b). The global correlation approaches zero near degree 120 showing there is not much benefit in extending the solution beyond degree 120 using MRO tracking data.

The spherical harmonic resolution of the gravity field can also be displayed spatially using the full unconstrained covariance matrix of the MRO120D solution. For each longitude and latitude, the gravity error spectrum is computed and compared to the expected gravity coefficient magnitude versus degree. The point where the error in the spectrum equals the signal gives the resolution or degree strength [e.g. Konopliv *et al.*, 1999]. Fig. 6 shows the resulting resolution for this gravity solution, and shows an improvement of at least 5 harmonic degrees versus the previous map of Konopliv *et al.* [2011].

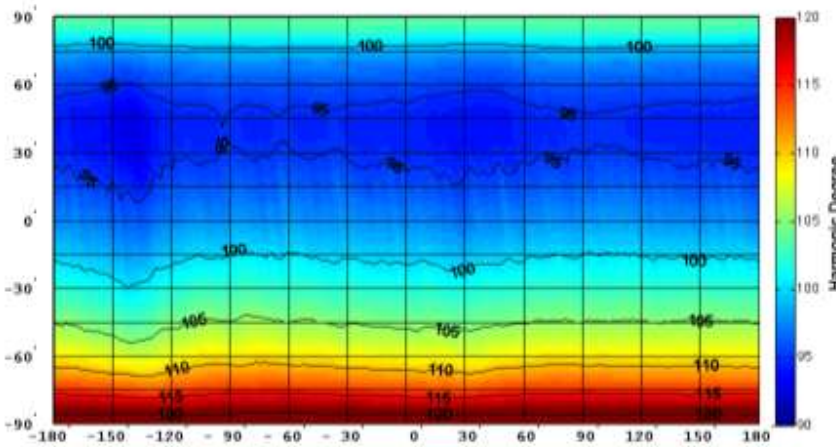


Figure 6. The resolution of the Mars gravity field MRO120D from the covariance matrix of the solution. The minimum resolution is harmonic degree 90 and improves over the south pole due to the lower altitude of the MRO orbit.

The solutions for other gravity parameters include the Mars Love number  $k_2=0.169\pm 0.006$ , Phobos  $GM=7.11\pm 0.05 \times 10^{-4} \text{ km}^3/\text{s}^2$ , and Deimos  $GM=9.5\pm 1.2 \times 10^{-5} \text{ km}^3/\text{s}^2$ . The Love number solution is the combined solution from all three orbiters with the uncertainty increased by a factor of two and is consistent but slightly lower than the previous determinations, in part, due to the rescaled orbiter SRIFs. The combined all orbiter solution for MRO110B is  $k_2=0.183$ , although the adopted Love number  $k_2=0.173\pm 0.009$  [Konopliv *et al.*, 2011] came from the MGS data only. The MRO110C combined solution is  $k_2=0.176$ . The Phobos mass determination comes from only long-term effects on the Mars orbiters without any close flyby tracking data from Viking or Mars Express. It is consistent with close flyby determinations of Phobos  $7.092 \times 10^{-4} \text{ km}^3/\text{s}^2$  [Jacobson and Lainey, 2013] with Viking, Phobos 2 and Mars Express data and  $7.084 \times 10^{-4} \text{ km}^3/\text{s}^2$  [Patzold *et al.*, 2013] from Mars Express. The Deimos  $GM$  from Jacobson and Lainey [2013] and Viking data is  $9.62 \pm 0.028 \times 10^{-5} \text{ km}^3/\text{s}^2$ .

The solution for the Mars orientation parameters is shown in Table 2 for the orbiter, lander and combined data sets. The continued improvement in the combined Mars gravity and orientation solutions is evident from the MRO110B, MRO110C, to MRO120D solutions, which include several years of Mars orbiter data in each subsequent solution. Since we now correlate the lander Doppler observations and scale the information arrays for each orbiter, the values and uncertainties of *Kuchynka et al.*, [2014] are comparable to the MRO120D solution. These solutions have consistent weighting of the orbiter and lander data except for an improved weighting of the MGS and Mars Odyssey orbiter data (a scaling of 10 instead of 15). The rotational pole parameter uncertainties improve by about a factor of two whereas the seasonal spin parameters improve by 10-20% since they are dominated by the Viking Lander contribution. Orientation parameters between the two approaches are mostly consistent within several standard deviations. The precession of Mars is consistent across orbiter and lander solutions with a combined value of  $-7608.3 \pm 2.1$  mas/yr.

Orientati on Paramete r	Kuchynka et al. (2014) Value/Error	MRO110B Value/Error	MRO110C Value/Error	MRO120D (Orbiter) Value/Error	MRO120D (Lander) Value/Error	MRO120D (All) Value/Error
$\psi_o$ (deg)	81.968379	81.9683722	81.9684072	81.9684029	81.9683310	81.9683988
	0.000009	0.000016	0.000010	0.0000054	0.0000450	0.0000043
$\dot{\psi}_o$ (mas/yr)	-7606.1	-7590.	-7613.5	-7610.1	-7611.4	-7608.3
	3.5	10.	5.2	2.7	7.3	2.1
$I_o$ (deg)	25.189383	25.1893792	25.1893863	25.1893855	25.1893772	25.1893823
	0.000005	0.000010	0.000006	0.0000031	0.0000129	0.0000026
$\dot{I}_o$ (mas/yr)	-1.	-4.1	-3.7	-3.4	-0.8	-2.0
	2.	6.3	3.1	1.3	3.5	1.1
$\phi_o$	133.386209	133.38462	133.38462	133.389562	133.386112	133.386277

(deg/day )						
	0.000043	(fixed)	(fixed)	0.025000	0.000105	0.000019
$\dot{\phi}_o$ (deg/day )	350.891985294 03	350.8919853 11	350.8919853 10	350.8919853 80	350.8919852 07	350.8919853
	0.000000006	0.000000012	0.000000007	0.000000003	0.000000013	0.000000003
$\phi_{c1} \phi_{s1}$ (mas)	$494 \pm 13$	$398 \pm 31$	$448 \pm 30$	$464 \pm 17$	$475 \pm 16$	$481 \pm 10$
	$-195 \pm 16$	$-222 \pm 41$	$-141 \pm 30$	$-140 \pm 17$	$-195 \pm 19$	$-155 \pm 12$
$\phi_{c2} \phi_{s2}$ (mas)	$-114 \pm 11$	$-110 \pm 31$	$-103 \pm 27$	$-101 \pm 16$	$-111 \pm 13$	$-103 \pm 9$
	$-105 \pm 10$	$-128 \pm 30$	$-133 \pm 26$	$-131 \pm 17$	$-82 \pm 14$	$-93 \pm 8$
$\phi_{c3} \phi_{s3}$ (mas)	$-34 \pm 9$	$7 \pm 26$	$-27 \pm 24$	$-6 \pm 15$	$-42 \pm 12$	$-35 \pm 8$
	$-1 \pm 8$	$-30 \pm 24$	$-10 \pm 25$	$-24 \pm 16$	$3 \pm 10$	$-3 \pm 7$
$\phi_{c4} \phi_{s4}$ (mas)	$-4 \pm 6$	$-16 \pm 22$	$-16 \pm 21$	$-9 \pm 15$	$-12 \pm 7$	$-10 \pm 6$
	$-22 \pm 7$	$6 \pm 22$	$-12 \pm 22$	$-22 \pm 15$	$-15 \pm 8$	$-8 \pm 6$

Table 2. Mars Orientation parameter solution from the MRO120D gravity field for orbiter data only, lander data only and combined. Other orientation parameters are held fixed with values given in Konopliv et al., 2011. The values from Kuchynka et al. (2014) are the combined orbiter and lander solution and incorporated results from MRO110C gravity solution. The uncertainties given are the formal uncertainties from the MRO120D solution, which are close to realistic errors since the lander data are whitened and the orbiter error covariances are rescaled. The errors for the MRO110B and MRO110C combined gravity and orientation solutions are the formal errors times 15. Note there is a typo in Table 2 of Kuchynka et al. (2014) giving an incorrect  $\dot{\phi}_o$ . The correct value is given in this table.

## 5. Conclusion

Several years of additional MRO and Mars Odyssey orbiter tracking data and MER Opportunity lander data have continued to improve the Mars gravity with higher resolution and more precise orientation parameters including precession, pole location, rotation rate and seasonal spin variations. The next incremental improvement in the Mars gravity field may come from the MAVEN Mars orbiter. MAVEN is in highly elliptic

orbit (4.5h period), but it may improve gravity over specific regions where there is low periapse coverage (~135 km). The next mission to significantly improve the Mars orientation will be InSight, a lander expected to arrive at Mars in 2018.

### Acknowledgements

The research described in this paper was carried out at the Jet Propulsion Laboratory, California Institute of Technology, under contract with the National Aeronautics and Space Administration.

### References

- Archinal, B. A., M. F. A'Hearn, E. Bowell, A. Conrad, G. J. Consolmagno, R. Courtin, T. Fukushima, D. Hestroffer, J. L. Hilton and G. A. Krasinsky, G. Neumann, J. Oberst, P. K. Seidelmann, P. Stooke, D. J. Tholen, P. C. Thomas, I. P. Williams, 2011. Report of the IAU Working Group on Cartographic Coordinates and Rotational Elements: 2009. *Celest. Mech. & Dyn. Astron.* 109, 101-135.
- Bierman, G. J., 1977. *Factorization Methods for Discrete Sequential Estimation*. Academic Press, New York.
- Folkner, W. M., C. F. Yoder, D. N. Yuan, E. M. Standish, R. A. Preston, 1997. Interior Structure and Seasonal Mass Redistribution of Mars from Radio Tracking of Mars Pathfinder. *Science*, 278, 1749-1752.
- Folkner, W. M., J. G. Williams, D. H. Boggs, R. S. Park, P. Kuchynka, 2014. The Planetary and Lunar Ephemeris DE430 and DE431. *IPN Progress Report 42-196*, Jet Propulsion Laboratory, Pasadena, CA.

- Heiskanen, W. A., and H. Moritz, 1967. *Physical Geodesy*. W. H. Freeman and Company, San Francisco and London.
- Jacobson, R. A., and V. Lainey, 2014. Martian satellite orbits and ephemerides. *Plan. & Sp. Sci.*, 102, 35-44.
- Kaula, W. M., 1966. *Theory of Satellite Geodesy*. Blaisdell, Waltham, MA.
- Konopliv, A. S., and W. L. Sjogren, 1995. The JPL Mars gravity field, Mars50c, based upon Viking and Mariner 9 Doppler tracking data. Publ. 95-5, Jet Propulsion Lab., Calif. Inst. of Technol., Pasadena, CA.
- Konopliv, A. S., W. B. Banerdt, and W. L. Sjogren, 1999. Venus Gravity: 180th Degree and Order Model. *Icarus*, 139, 3–18.
- Konopliv, A. S., C. F. Yoder, E. M. Standish, D. N. Yuan, W. L. Sjogren, 2006. A global solution for the Mars static and seasonal gravity, Mars orientation, Phobos and Deimos masses, and Mars ephemeris. *Icarus*, 182, 23-50.
- Konopliv, A. S., S. W. Asmar, W. M. Folkner, O. Karatekin, D. C. Nunes, S. E. Smrekar, C. F. Yoder, M. T. Zuber, 2011. Mars High Resolution Gravity Fields from MRO, Mars Seasonal Gravity, and Other Dynamical Parameters. *Icarus*, 211, 401-428.
- Konopliv, A. S., R. S. Park, D.-N. Yuan, S. W. Asmar, M. M. Watkins, J. G. Williams, E. Fahnestock, G. Kruizinga, M. Paik, D. Strekalov, N. Harvey, D. E. Smith, M. T. Zuber, 2013. The JPL Lunar Gravity Field to Spherical Harmonic Degree 660 from the GRAIL Primary Mission, *J. Geophys. Res.*, 118, doi: 10.1002/jgre.20097.
- Kuchynka, P., W. M. Folkner, A. S. Konopliv, T. J. Parker, R. S. Park, S. Le Maistre, V. Dehant, 2014. New constraints on Mars rotation determined from radiometric tracking of the Opportunity Mars Exploration Rover. *Icarus*, 229, 340-347.

- Lambeck, K., 1988. *Geophysical Geodesy*. Clarendon Press, Oxford.
- Lawson, C. L., and R. J. Hanson, 1995. *Solving Least Squares Problems*. SIAM Classics in Applied Mathematics, Vol. 15, Society for Industrial and Applied Mathematics, Philadelphia.
- Lemoine, F. G., D. E. Smith, D. D. Rowlands, M. T. Zuber, G. A. Neumann, D. S. Chinn, 2001. An improved solution of the gravity field of Mars (GMM-2B) from Mars Global Surveyor. *J. Geophys. Res.*, 106, 23359-23376.
- Marty, J. C., G. Balmino, P. Rosenblatt, J. Duron, S. LeMaistre, A. Rivoldini, V. Dehant, T. Van Hoolst, 2009. Martian gravity field model and its time variations from MGS and Odyssey data, *Plan. & Space Sci.*, doi: 10.1016/j.pss.2009.01.004.
- Patzold, M., T. Andert, R. Jacobson, P. Rosenblatt, V. Dehant, 2014. *Plan. & Sp. Sci.*, 102, 86-94.
- Semenov, B.V., L.S. Elson, C.H. Acton, 1998. MARS GLOBAL SURVEYOR SPICE KERNELS V1.0, MGS-M-SPICE-6-V1.0, NASA Planetary Data System.
- Semenov, B.V., L.S. Elson, C.H. Acton, 2004. ODYSSEY SPICE KERNELS V1.0, ODY-M-SPICE-6-V1.0, NASA Planetary Data System.
- Semenov, B.V., and C.H. Acton, 2007. MARS RECONNAISSANCE ORBITER SPICE KERNELS V1.0, MRO-M-SPICE-6-V1.0, NASA Planetary Data System.
- Smith, D. E., F. J. Lerch, R. S. Nerem, M. T. Zuber, G. B. Patel, S. K. Fricke, and F. G. Lemoine, 1993. The gravity model for Mars: Goddard Mars Model I. *J. Geophys. Res.*, 98, 20,871-20,889.
- Smith, D. E., W. L. Sjogren, G. L. Tyler, G. Balmino, F. G. Lemoine, A. S. Konopliv, 1999. The Gravity Field of Mars: Results from Mars Global Surveyor. *Science*, 286,

94-97.

- Smith, D. E., M. T. Zuber, H. V. Frey, J. B. Garvin, J. W. Head, D. O. Muhleman, G. H. Pettengill, R. J. Phillips, S. C. Solomon, H. J. Zwally, W. B. Banerdt, T. C. Duxbury, M. P. Golombek, F. G. Lemoine, G. A. Neumann, D. D. Rowlands, O. Aharonson, P. G. Ford, A. B. Ivanov, C. L. Johnson, P. J. McGovern, J. B. Abshire, R. S. Afzal, X. Sun, 2001. Mars Orbiter Laser Altimeter: Experiment summary after the first year of global mapping of Mars. *J. Geophys. Res.*, *106*, 23689-23722.
- Woo, R., Armstrong, J. W., 1979. Spacecraft radio scattering observations of the power spectrum of electron density fluctuations in the solar wind. *J. Geophys. Res.*, *84*, 7288–7296.
- Yoder, C. F., A. S. Konopliv, D. N. Yuan, E. M. Standish, W. M. Folkner, 2003. Fluid Core Size of Mars from Detection of the Solar Tide. *Science*, *300*, 299-303.
- Yuan, D. N. W. L. Sjogren, A. S. Konopliv, A. B. Kucinskas, 2001. Gravity field of Mars: A 75th Degree and Order Model. *J. Geophys. Res.*, *106*, 23377-23401.
- Zuber, M. T., F. G. Lemoine, D. E. Smith, A. S. Konopliv, S. E., Smrekar, S. W. Asmar, 2007. Mars Reconnaissance Orbiter Radio Science Investigation. *J. Geophys. Res.*, *112*, E05S07, doi:10.1029/2006JE002833.